Int. J. Nano Dimens., 9 (4): 346-356, Autumn 2018

ORIGINAL ARTICLE

Influence of reaction parameters on crystal phase growth and optical properties of ultrasonic assisted Hydro-and solvothermal synthesized sub-micrometer-sized CdS spheres

*Leila Kafi-Ahmadi[1], *, Robabe Mohammadzadeh-Hesar[1], Shahin Khademinia[2]*

[1]*Department of Inorganic Chemistry, Faculty of Chemistry, Urmia University, Urmia, Iran*

[2]*Department of Inorganic Chemistry, Faculty of Chemistry, Semnan University, Semnan 35351-19111, Iran*

Received 11 March 2018; revised 29 May 2018; accepted 07 June 2018; available online 09 June 2018

Abstract

Sub-micrometer-sized CdS spheres were synthesized by hydrothermal and solvothermal reactions using $Cd(NO_3)_2.4H_2O$ and CH_4N_2S raw materials at a constant stoichiometric 1 : 2, Cd : S molar ratio. Various conditions such as solvent type (water and/or ethanol), reaction time and temperature were examined for the synthesis of the targets. The synthesized materials were characterized by powder X-ray diffraction (PXRD) technique and fourier-transform infrared (FTIR) spectroscopy. Crystal structure study was performed in a comparison mode to investigate the crystalline phase purity and growth of the obtained CdS materials when the reaction conditions were changed. The PXRD data indicated that the as-synthesized materials were crystallized well in a hexagonal crystal system with the space group $P6_3mc$. However, the crystal phase growth study showed that a cubic crystal system of CdS was obtained as a second crystal phase in the mixture. The morphologies of the synthesized materials were studied by field emission scanning electron microscopy (FESEM) technique. The data showed that the reaction solvent had a critical influence on the morphology of the obtained materials. Ultraviolet-visible spectra showed that the synthesized CdS materials had strong light absorption in the ultraviolet-visible light regions. The calculated direct optical band gap energies of the obtained materials were in the ranges of 1.90-2.30 eV.

Keywords: *Cadmium Sulfide; Crystal Phase; Hydrothermal; Optical Property; Purity.*

How to cite this article

Kafi-Ahmadi L, Mohammadzadeh-Hesar R, Khademinia S. Influence of reaction parameters on crystal phase growth and optical properties of ultrasonic assisted Hydro-and solvothermal synthesized sub-micrometer-sized CdS spheres. Int. J. Nano Dimens., 2018; 9 (4): 346-356.

INTRODUCTION

Among the II-VI semiconductors, cadmium sulphide (CdS) is one of the most important wide gap semiconductors with $E_g \approx 2.5$ eV for the bulk hexagonal wurtzite phase and $E_g \approx 3.53$ eV for the bulk cubic phase. In particular, many researchers have carried out studies on CdS because of its numerous applications as photocatalyst, solar cells and light-emitting diodes [1-4], piezoelectric [5], optoelectronic [6], etc. Different methods have been reported for the preparation of CdS materials, such as solid-state methods [7,8], solvothermal [9-11], precipitation [12-16], microwave-assisted solvothermal [17], liquid-crystal templating [18], calcinations of Cd-thiolates [19], vapor–liquid–solid [20], template [21], aqueous-solution process [22], thermal evaporation [23], chemical vapor deposition [24], microwave irradiation [25], hydrothermal [26-33], electrochemical [34], Spray-Pyrolysis [35], direct vapor transport [36], electrodeposition [37], laser ablation [38], microemulsion [39], microwave [40], sonochemical [41], microwave assisted sol-gel [42] methods, etc. Among various techniques, hydrothermal reaction is a powerful method providing a material with high crystal phase purity, nano-sized particles and controlled stoichiometry of CdS powder [43, 44]. Hydrothermal name has

* Corresponding Author Email: *l.kafiahmadi@urmia.ac.ir*

Greek origin which is composed of two words 'hydros' meaning water and 'thermos' meaning heat and can be defined as any heterogeneous reaction in the presence of aqueous solvents or mineralizes under high pressure and temperature conditions to dissolve and recrystallize (recover) materials that are relatively insoluble under ordinary conditions. This method can be as an important tool for advanced materials processing and used in preparation of mono dispersed and highly homogeneous nanoparticles and nano-hybrid and nanocomposite materials. The mentioned method has potential advantages of relatively low cost, high purity, energy saving, nucleation control, avoidance of pollution, high dispersion, high rate of reaction, shape control, and low temperature operations in the presence of the solvent [43].

In the present study, ultrasonic assisted hydrothermal and solvothermal routs are applied for the synthesis of sub-micron structured CdS powders using $Cd(NO_3)_2.4H_2O$ and CH_4N_2S raw materials. Different reaction conditions such solvent type, time and temperature are studied for their influence on the purity, crystal phase type and growth of the synthesized materials. The crystallographic data are extracted and compared to study the crystallite size, crystal phase purity and growth. The optical properties of the obtained materials are also investigated by UV-Vis and FTIR spectroscopies.

EXPERIMENTAL

Materials and instruments

All chemicals including $Cd(NO_3)_2.4H_2O$, CH_4N_2S, NH_4OH, deionized distilled water and ethanol were of analytical grade, obtained from commercial sources (Merck Company) and used without further purifications. Phase identifications were performed on a powder X-ray diffractometer D5000 (Siemens AG, Munich, Germany) using CuK_α radiation. The morphology of the obtained materials was examined with a field emission scanning electron microscope (Hitachi FE-SEM model S-4160). FTIR spectra were recorded on a Tensor 27 spectrometer (Bruker Corporation, Germany). Absorption spectra were recorded on a UV-visible spectrophotometer model-UV-1650 PC (Shimadzu, Japan). Cell parameter refinement was reported by celref software version 3 (Laboratoire des Materiaux et du Génie Physique de l'Ecole Supérieure de Physique de Grenoble). Ultrasonic device (SOLTEC, Italy) with the power of 305 W was used.

Synthesis of CdS samples

In a typical experiment, 3.084 g (10.0 mmol) of $Cd(NO_3)_2.4H_2O$ (Mw = 308.4 g mol^{-1}) was dissolved in a 15 mL of solvent (deionized distilled water) (solution 1). In another beaker, 1.522 g (20 mmol) of CH_4N_2S (Mw=76.0 g mol^{-1}) was dissolved in a 15 mL of the mentioned solvent (solution 2). Afterwards, the solution 2 was added to the solution 1 drop wise while stirring. The pH value of the final solution was adjusted in the range of 9-10 using NH_4OH solution. The obtained solution was agitated further for 1 h and then ultrasonicated for 1 h. The resultant solution was transferred into a 100-mL Teflon lined stainless steel autoclave. The autoclave was sealed and treated thermally at 120°C for 48 h (S_1), 150°C for 48 h (S_2), 150°C for 72 h (S_3), 150°C for 96 h (S_4), and 180°C for 48 h (S_5). When the reaction was completed, the autoclave was cooled to room temperature by quenching with water immediately. The prepared powder was washed with distilled water and dried at 80°C for 3 h under normal atmospheric condition. An orange color powder was collected.

For the synthesis of S_6 and S_7, the synthesis procedure explained for S_1 was followed. However, in this case, the solvent type is ethanol and the reaction temperature is 180°C for 48 h (S_6) and 72 h (S_7).

For the synthesis of S_8, S_9 and S_{10}, the synthesis procedure explained for S_1 was used. In this case, the solvent type is a 1 : 1 volumetric mixture of water and ethanol. The reaction temperature is 180°C for 48 h (S_8), 72 h (S_9) and 96 h (S_{10}).

RESULTS AND DISCUSSIONS

Characterization

The PXRD patterns of the obtained materials are classified and shown in Figs. 1-4. The data show that all the diffraction patterns match exactly to the hexagonal wurtzite-structure with the space group $P6_3mc$ (JCPDS Card No. 41-1049). The diffraction peaks are indexed to (1 0 0), (0 0 2), (1 0 1), (1 0 2), (1 1 0), (1 0 3), (1 1 2), (2 0 3) and (2 1 1) diffraction planes of the wurtzite CdS crystalline phase, respectively. The data show that the peaks at (111) (broad and overlapped peak with the (0 0 2) peak in the hexagonal crystal system), (2 0 0), (4 0 0) and (3 3 1) diffraction planes are corresponded to the cubic CdS crystal

system (space group: F-43m, JCPDS Cards, No. 10-0454). To make a useful and comprehensive comparison study, the PXRD patterns are classified based on reaction time, temperature and solvent type. Fig. 1 a-c shows the PXRD patterns of the obtained samples when the solvent type is water and the reaction time is 48 h. The figure shows that when the reaction temperature is 120 °C, there is an obvious impurity cubic CdS peak position at 2θ=31° in the mixture. The peaks with the h k l values of 200, 112 and 201 at about 50 to 55° are combined and become a single peak that is attributed to the cubic CdS crystal phase. However, with increase the reaction time to 150 and then 180 °C, the impurity peak is disappeared and the peak corresponded to the wurtzite crystal system (1 0 1) is grown considerably. In this case, the mentioned three peaks are appeared as three separated peaks showing the good crystallinity of hexagonal crystal system.

Fig. 2 a-c shows the PXRD patterns of the obtained materials when the reaction solvent is H_2O, reaction temperature is 150°C and reaction times change from 48 h to 96 h. The data show that there is no considerable change in the crystal phase purity when the reaction time increased. However, the counts values show that when the reaction time is 72 h, the crystal phase growth is retrograded. The phenomenon is maybe because of changing the cubic crystal phase to the hexagonal crystal system when the reaction time is 72 h. This can be seen from increasing the growth

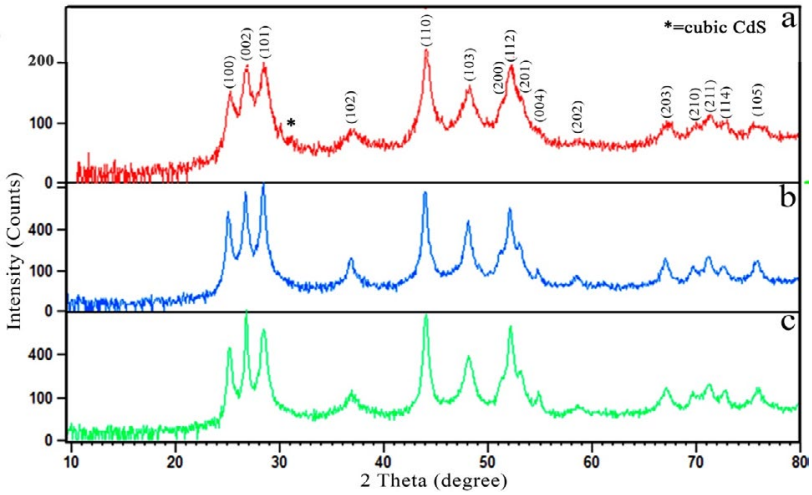

Fig. 1. PXRD patterns of a) S_1, b) S_2 and c) S_5.

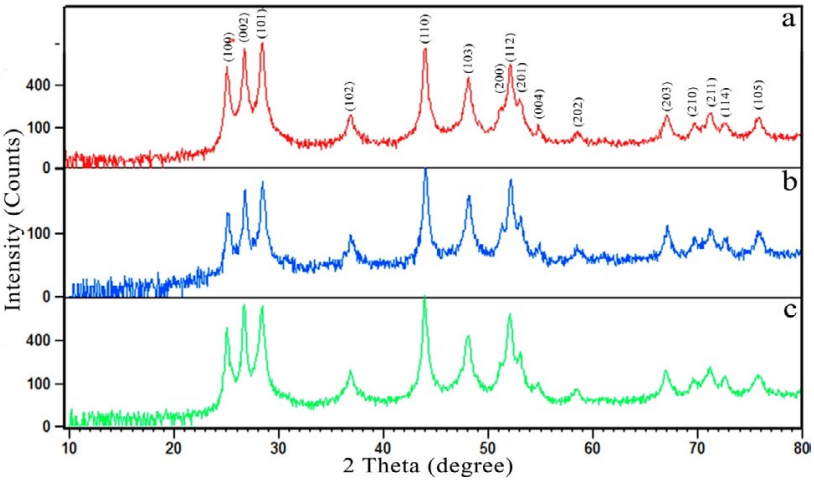

Fig. 2. PXRD patterns of a) S_2, b) S_3 and c) S_4.

of the peak at (1 0 1) compared to the overlapped peak (0 0 2). However, the crystal phase growth is improved again when the reaction time was increased to 96 h. In other words, when the crystal phase change is completed, the hexagonal crystal phase is grown again with increase the reaction time to 96 h.

Fig. 3 a-c shows the PXRD data of the obtained materials at 180°C for 48, 72 and 96 h. The solvent is a mixture of 1 : 1, H2O : Ethanol. The PXRD data show that the materials have a high crystalline hexagonal CdS phase. As it can be seen from the data, the mixture of H_2O and ethanol as the reaction solvent has a considerable influence on the crystal phase growth of the target. However, it is clear that when the reaction time is 48 h, there is an impurity peak corresponded to the cubic CdS crystal system. When the reaction time is increased to 96 h, the cubic impurity, marked with *, is disappeared. But the peak intensity at (0 0 2) is increases compared to the peak at (1 0 1). This indicates that increasing the reaction time to 96 h changes the crystal phase stability from hexagonal to cubic crystal system.

Fig. 4 a-d shows the PXRD patterns of obtained materials when the solvents are H_2O and a 1 : 1 mixture of H_2O : Ethanol, at 180°C for 48 h; and ethanol, at 180°C for 48 and 72 h. The data show that when the solvent is ethanol and the mixture of H_2O and ethanol, the material is composed of the mixtures of hexagonal [7-10] and cubic [46-48] CdS crystal phases. But, H_2O can advance the

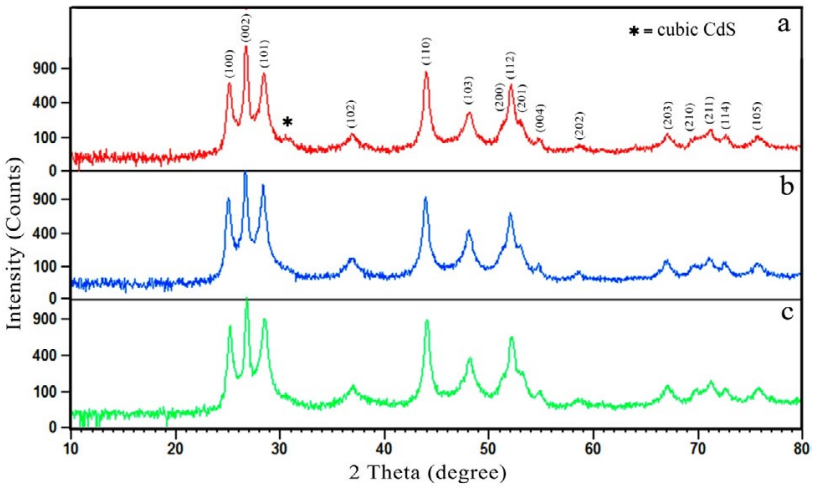

Fig. 3. PXRD patterns of a) S_8, b) S_9 and c) S_{10}.

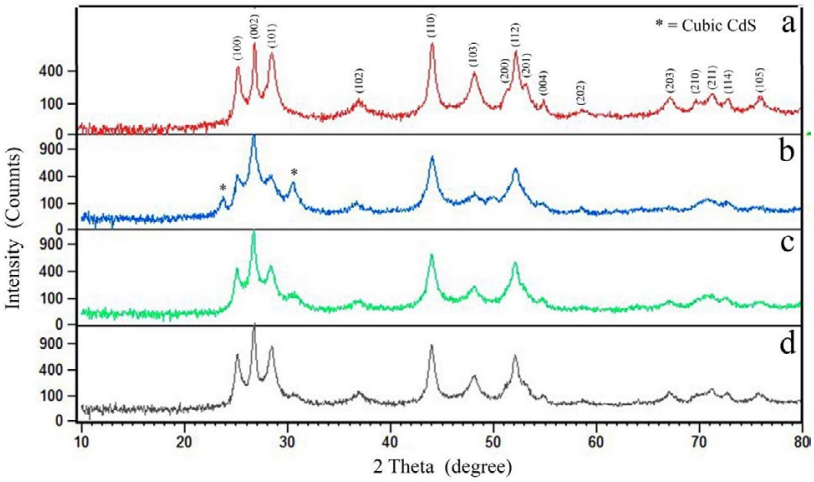

Fig. 4. PXRD patterns of a) S_5, b) S_6, c) S_7 and d) S_8.

process in a way that no obvious impurity phase is present in the PXRD pattern.

To study the solvent type, reaction time and temperature influences on the crystal phase purity and growth, the phase composition was calculated from the integrated intensities of the wurtzite (1 0 0) peak (2θ ≈ 25.2 °) and the overlapping sphalerite (1 1 1) and wurtzite (0 0 2) peaks (2θ ≈ 26.8◦). In the mixed phase products, the weight fraction of wurtzite (F_w) can be estimated as below:

$$F_w = \frac{R}{K} - (kk' - 1)R$$

Where R represents the intensity ratio of wurtzite peak (1 0 0) to the overlapping peak (measured), k'= 0.825 is the intensity ratio of the wurtzite peak (0 0 2) to peak (1 0 0) (standard pattern), and k = 0.341 is the intensity ratio of the wurtzite peak (1 0 0) to the sphlerite peak (1 1 1) (standard pattern) [44].

According to the data, Fw value for S_3, S_6, S_9 and S_{10} is below 2. The observation indicates that reaction time is a main factor on the wurtzite crystal phase purity. The lowest amounts are for S_9 and S_{10}. This shows that ethanol as a reaction solvent cannot force the reaction in an effective way to produce a purer wurtzite crystal phase. However, when the solvent is H_2O and the reaction temperature is 150 °C for S_2 and S_5, Fw value is maximized.

Table 2 shows the crystallite size data of the obtained materials calculated by Scherrer equation:

$$D = \frac{K\lambda}{B_{\frac{1}{2}} cos\theta}$$

In this equation, D is the entire thickness of the crystalline sample, λ is the X-ray diffraction wavelength (0.154 nm), K is Scherrer constant (0.9), $B_{1/2}$ (rad) of FWHM is the full width at half its maximum intensity and θ is the half diffraction angle at which the peak is located. The data reveal that when the reaction time and temperature are 48 h and 120°C, respectively, and the solvent type is H_2O (S_1), the crystallite size is largest compared to the other synthesized samples. Surprisingly, the table shows that the crystallite size is decreased when the reaction time and temperature are increased to 96 h and 180°C, respectively. Besides, the data indicate that the crystallite sizes of S_1-S_5, when the solvent is H_2O, are larger than those of the other types of the solvents.

The value of the dislocation density (δ(lines/m^2)× 10^{14}) which is related to the number of defects in the crystal was calculated from the average values of the crystallite size (D (nm)) by the relationship (3.3) given below:

$$\delta = \frac{1}{D^2}$$

Table 2. Crystallite size data of the as-synthesized materials.

Sample	$I_{(100)}$	$I_{(002)}$	$I_{(101)}$	$I_{(100)}/I_{(002)}$	$I_{(101)}/I_{(002)}$	Fw
S_1	220	371	378	0.592992	1.018868	2.164421
S_2	567	805	940	0.704348	1.167702	2.570870
S_3	438	867	637	0.505190	0.734717	1.843944
S_4	167	271	314	0.616236	1.158672	2.249261
S_5	485	750	745	0.646667	0.993333	2.360335
S_6	640	1327	786	0.482291	0.592313	1.760362
S_7	893	1447	1182	0.617139	0.816862	2.252557
S_8	740	1208	856	0.612583	0.708609	2.235928
S_9	401	1215	397	0.330041	0.326749	1.204650
S_{10}	429	1199	456	0.357798	0.380317	1.305963

Table 1. Phase composition properties of the obtained samples.

Sample	2θ	cos(θ)	$B_{1/2}$	D	δ	ε
S_1	43.98	0.9272	0.004120	36	7.716049	0.955016
S_2	43.9091	0.9275	0.005150	29	11.89061	1.194156
S_3	43.8749	0.9276	0.006179	24	17.36111	1.432910
S_4	43.9303	0.9274	0.005373	28	12.75510	1.245730
S_5	43.9801	0.9272	0.005150	29	11.89061	1.193770
S_6	43.9622	0.9273	0.006866	22	20.66116	1.591710
S_7	43.8864	0.9276	0.006866	22	20.66116	1.592225
S_8	44.008	0.9272	0.006866	22	20.66116	1.591539
S_9	44.0189	0.9272	0.006866	22	20.66116	1.591539
S_{10}	44.0132	0.9272	0.006866	22	20.66116	1.591539

The strain ($\varepsilon \times 10^{-3}$) values were determined with the use of the following formula:

$$\varepsilon = \frac{\beta_{hkl}\, cos\theta}{4}$$

The data show that the dislocation density and strain values are depend on the crystallite size and FWHM values. The data show that the values were increased when the crystal sizes were decreased.

The crystallographic data of the obtained samples were calculated and compared using the peak with the miller indices 110 corresponded to the hexagonal CdS crystal system. The data are summarized in Table 3.

The below equations are used to calculate the d values:

$$n\lambda = 2d\, sin\theta$$

And

$$\frac{1}{d^2} = \frac{4(h^2 + hk + k^2)}{3a^2} + \frac{l^2}{c^2}$$

Using the peak with the (h k l) value of (1 1 0), the relation is as below:

$$\frac{1}{d^2} = \frac{8}{3a^2}$$

With simplifying the above equation, we obtain:

$$d = \sqrt{\frac{3}{8}}\, a$$

Besides, the unit cell volume can be obtained from the bellow formula:

$$V = \frac{\sqrt{3}}{2} c^2 a$$

Where a and c are the lattice parameters calculated by celref software and V is the cell volume.

The obtained data show that the calculated d values by Bragg equation (2) and (3) are not so in accordance with each other's. The difference is 0.46 Å. The difference is maybe due to uncertainty of the used cell parameter in eq.3 and the 2θ value used in eq.2. The uncertainty is obvious from the high dislocation density and strain values.

Morphology analysis

Fig. 5 shows the FESEM images of S_1-S_5. The images of S_1, S_2 and S_5 show that when the reaction time is 48 h, increasing the reaction temperature has no significant effect on the morphology of the targets. The data show that the material is composed of particle and also sphere structures. It is obvious from the images that when the reaction temperature is 150 °C, indicated with a, b and c, produces the material with almost particle morphology. However, when the reaction temperature is 120 and 180°C, the morphology of the targets is large size sphere.

Fig. 6 shows the FESEM images of S_6 and S_7. The images show that ethanol as the reaction solvent has an effect on the homogeneity of the obtained target. It is clear that the morphology homogeneity is better compared to S_1-S_4.

Fig. 7 shows the FESEM images of S_8 to S_{10}. The images show that when the reaction time is 48 h, the morphology is almost particle. However, the morphology becomes a mixture of particle and micro sphere when the reaction time is increased to 96 h.

All the FESEM images reveal that morphology of the targets depends on the solvent type and reaction time, considerably. If the morphology of highly homogeneous particle is desired, so the reaction procedure for the synthesis of S_2 and S_8 is applicable. However, when the material with sphere morphology is needed, the process for the synthesis of S_1, S_5, S_9 and S_{10} can be used.

Table 3. Lattice parameters and inter planar spacing data of the obtained materials.

Sample	a (Å)	c (Å)	d_{Bragg}(Å)	$d_{Cal.}$ (Å)	$V_{Cal.}$ (Å^3)
S_1	4.1154	6.6456	2.05860	2.520271	157.3977
S_2	4.1211	6.6795	2.06206	2.523762	159.2278
S_3	4.1262	6.6820	2.06357	2.526885	159.5442
S_4	4.1137	6.6912	2.05939	2.519230	159.4992
S_5	4.1119	6.6810	2.05887	2.518128	158.9437
S_6	4.1144	6.6863	2.05967	2.519659	159.2928
S_7	4.1213	6.6925	2.06305	2.523884	159.8560
S_8	4.1106	6.6811	2.05796	2.517331	158.8982
S_9	4.1073	6.7103	2.05715	2.515311	160.1615
S_{10}	4.1114	6.7022	2.05741	2.517821	159.9346

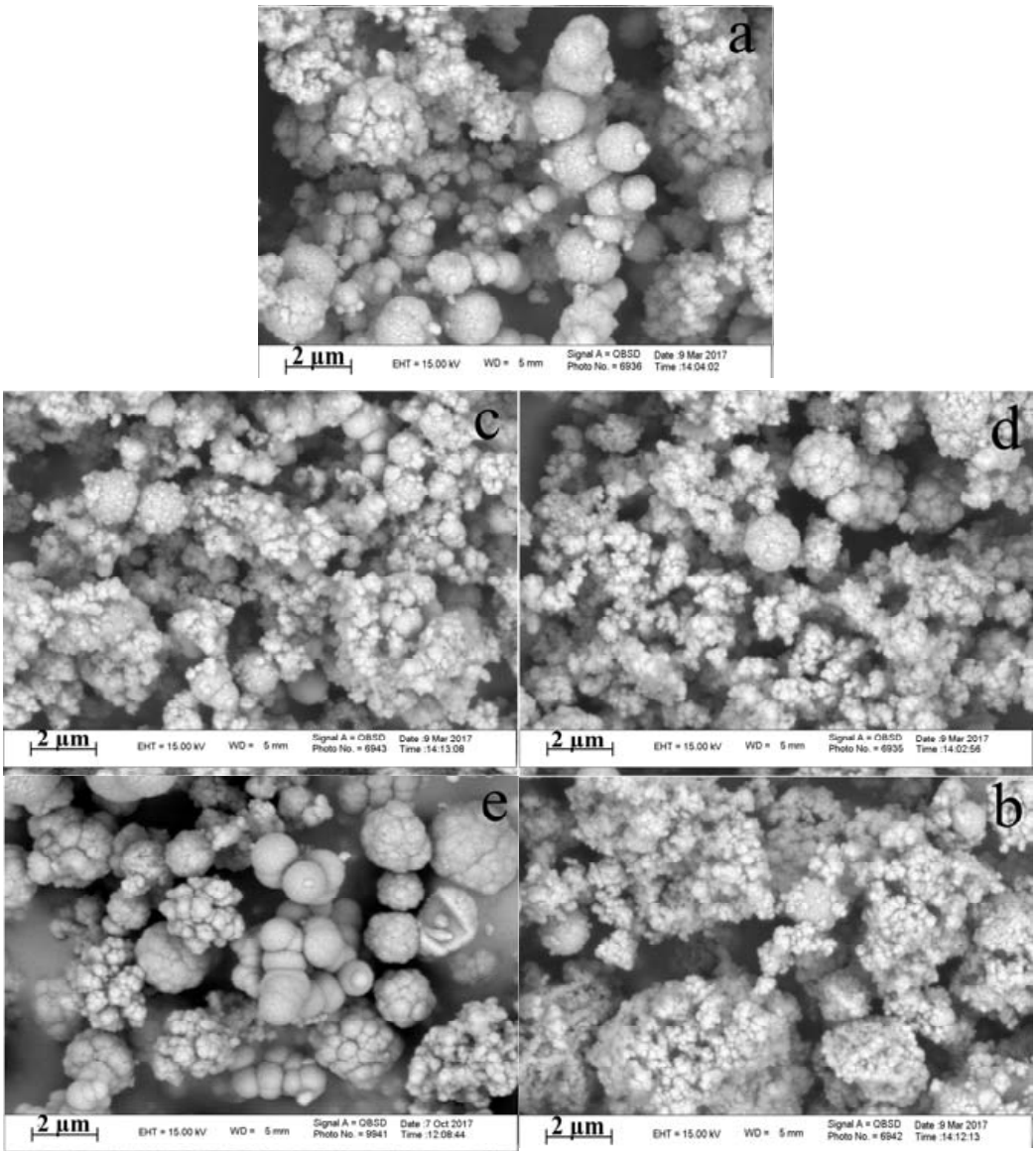

Fig. 5. FESEM images of a) S_1, b) S_2, c) S_3, d) S_4 and e) S_5.

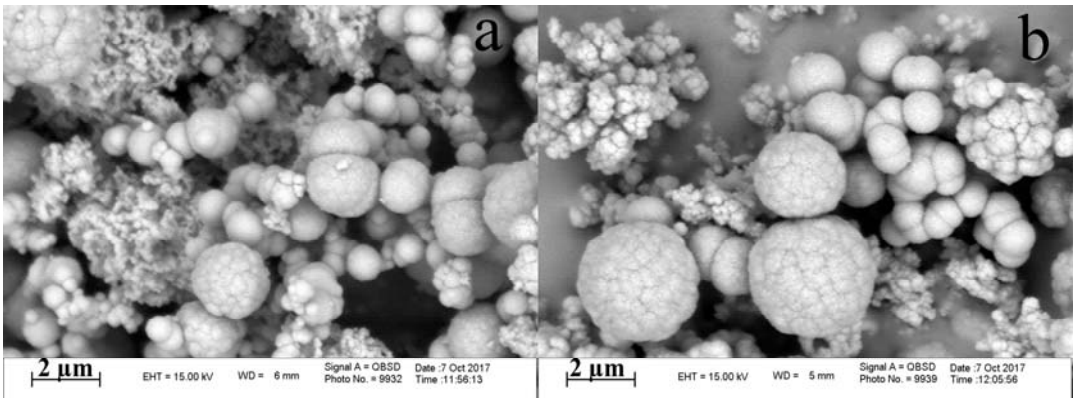

Fig. 6. FESEM images of a) S_6 and b) S_7.

Optical properties

UV-Vis spectra and the calculated direct optical band gap energies of the CdS materials obtained from the absorption spectra are shown in Figs. 8 a-c and 9 a-c, respectively. According to the results of Pascual *et al.* [49], the relation between the absorption coefficient and incident photon energy can be written as $(\alpha h\nu)^2 = A(h\nu - E_g)$, where A and E_g are a constant and the direct band gap energy, respectively. Direct band gap energies were evaluated from extrapolating the linear part of the curve to the energy axis.

Fig. 9 a-c shows that the direct optical band gaps are 2.15, 1.98, 2.23, 2.13 and 1.95 eV for S_1, S_2, S_3, S_4 and S_5, respectively.

The calculated band gap energies for S_1, S_2 and S_5 in Fig. 9 a show that increasing the reaction temperature at a constant reaction time decreases the band gap energy values. The data show that when the reaction time and temperature are 48 h and 180°C, the smallest band gap value is achived. Fig. 9 b shows that the direct optical band gap energies are 2.23 and 2.17 eV for S_6 and S_7, respectively. The data show that increasing the

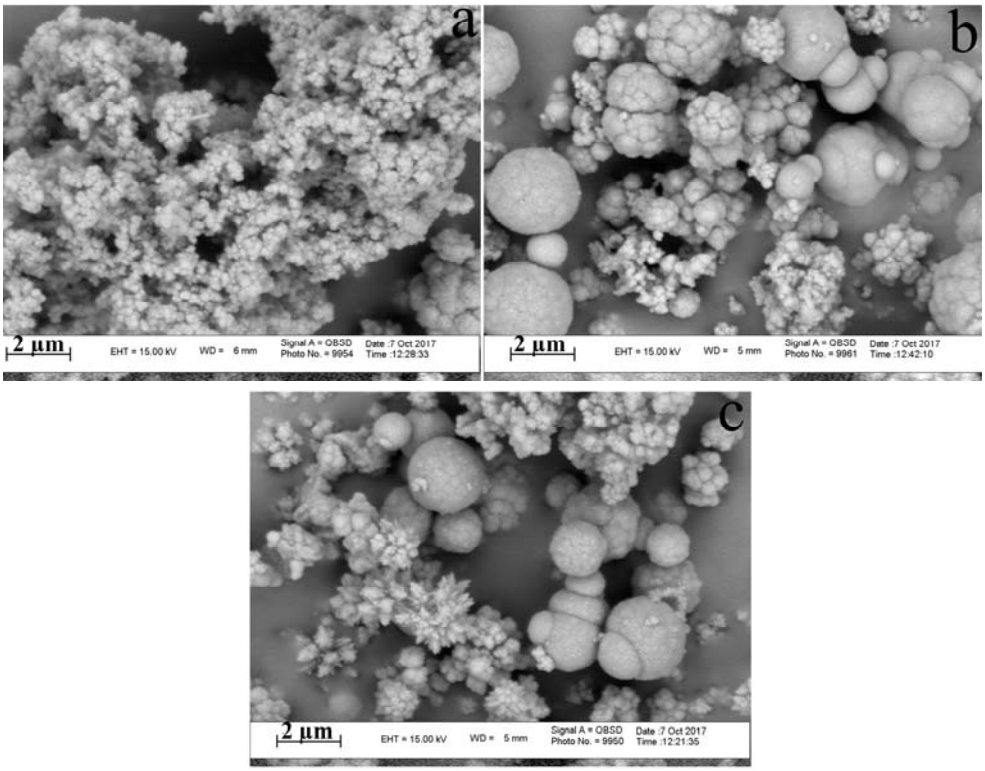

Fig. 7. FESEM images of a) S_8, b) S_9 and c) S_{10}.

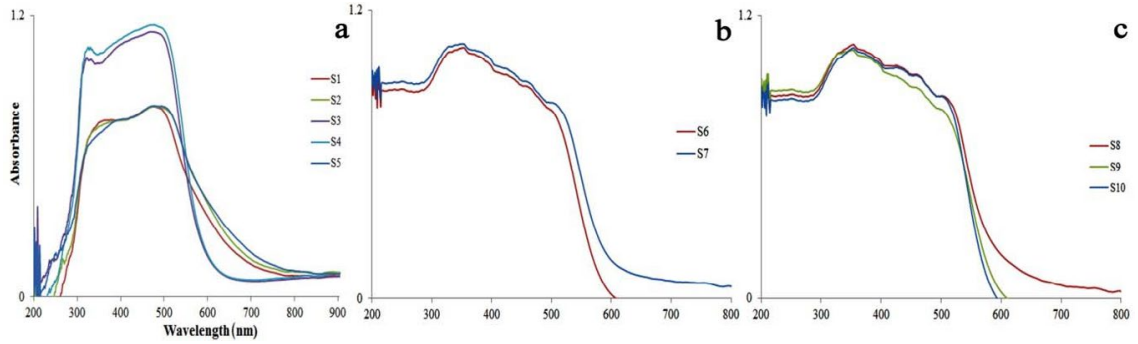

Fig. 8. UV-Vis absorption spectra of the obtained samples where a) S_1-S_5, b) S_6-S_7 and c) S_8-S_{10}.

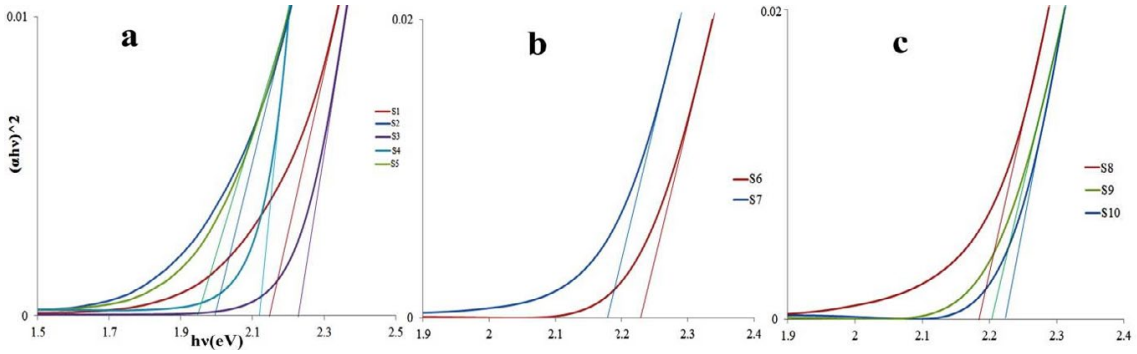

Fig. 9. Direct optical band gap energies of the obtained samples where a) S_1-S_5, b) S_6-S_7 and c) S_8-S_{10}.

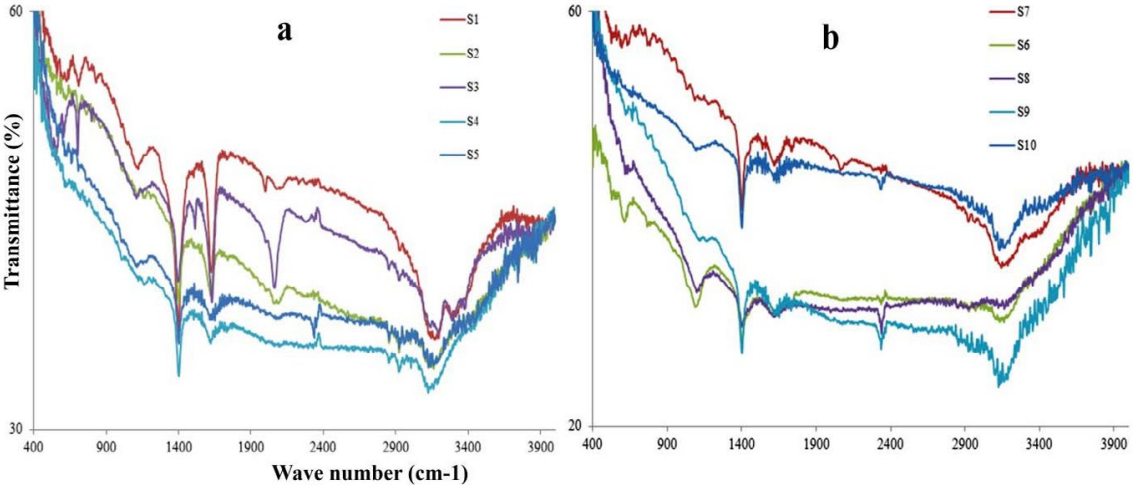

Fig. 10. FTIR spectra of the obtained materials where a)S_1-S_5 and b)S_6-S_{10}.

reaction time at a constant reaction temperature, 180 °C, with ethanol as the solvent, decreases the band gap energy. This trend is in agreement with that for S_1-S_5.

Fig. 9 c shows that the direct optical band gap energies are 2.18, 2.20 and 2.22 eV for S_8, S_9 and S_{10}, respectively. It is obvious that increasing the reaction time at 180°C increases the band gap energy.

The band gap energy change behaviors indicate that reaction solvent has a critical influence on the optical band gap of the obtained materials. So, because lower optical band gap energy is favored for the catalytic applications, it is a useful guide for the synthesis of the desired CdS material. In the case, H_2O as the reaction solvent is a good medium for the synthesis of the obtained target.

Fig. 10 a and b shows the FTIR spectra of the obtained samples. There are some peaks at around 670, 705, 1074, 1394, 1510, 1577, 2050, 2327, 2906, 3103 and 3294 cm^{-1}. The peaks at 670 and 705 cm^{-1}, are assigned to Cd–S stretching vibrations [16]; the absorption peak at 1394 cm^{-1} is corresponded to S-C stretching vibration; the peaks at 1510 and 1577 cm^{-1} are assigned to stretching vibration of N-H in thiourea compound [16]; the very weak peak at 2906 cm^{-1} is attributed to Cd-O stretching vibration [50]; the peak at 3103 and 3294 are assigned to N-H stretching vibrations [27, 47, 51].

CONCLUSION

Ultrasonic assisted hydrothermal and solvothermal syntheses of CdS micro spheres were explored. Various conditions such as solvent type, reaction time and temperature were investigated using PXRD data for their influences on the crystal phase growth, purity and type of the as-synthesized materials. The phase composition data showed that when the reaction solvent was

H_2O, there was a surprisingly tendency to the hexagonal CdS crystal phase. The data showed that when the solvent was a mixture of H_2O and ethanol (S_8-S_{10}), the reaction was proceeded in a way that the solvent acted in a reverse order compared to H_2O reaction solvent (S_1-S_5) and the main crystal phase stability, hexagonal crystal structure, was decreased when the reaction time was increased. Besides, the crystallite size data showed that the sizes of the targets were smallest when the mixture of H_2O and ethanol was used as the reaction solvent. FESEM images data revealed that the morphology of the targets depended on the solvent type and reaction time, considerably. If highly homogeneous particle morphology was desired, the reaction procedure for the synthesis of S_2 and S_8 was applicable. However, when the material with sphere morphology was needed, the process for the synthesis of S_1, S_5, S_9 and S_{10} could be used. The direct optical band gap energy changes were studied and related to the reaction parameters. The data showed that the smallest band gap energy was achieved when the reaction solvent was H_2O and the reaction time and temperature were 48 h and 180°C. At the end, the data showed that the reaction condition for the synthesis of S_5 was better than the others when purer crystal phase and low optical band gap energy was desired. However, when smaller crystallite size and high crystal growth were needed, the reaction conditions for the synthesis of S_{10} were useful.

CONFLICT OF INTEREST

The authors declare that there are no conflicts of interest regarding the publication of this manuscript.

REFERENCES

[1] Zhao J., Bardecker J. A., Munro A. M., Liu M. S., Niu Y., Ding I. K., Luo J., Chen B., Jen A. K., Ginger D. S., (2006), Efficient CdSe/CdS quantum dot light-emitting diodes using a thermally polymerized hole transport layer. *Nano Lett.* 6: 463-470.

[2] Shi J., Yan X., Cui H., Zong X., Fu M., Chen S., Wang L., (2012), Low-temperature synthesis of CdS/TiO_2 composite photocatalysts: Influence of synthetic procedure on photocatalytic activity under visible light. *J. Mol. Catal. A: Chem.* 356: 53-60.

[3] Zhang J., Yu J., Jaroniec M., Gong J. R., (2012), Noble metal-free reduced graphene oxide-$Zn_xCd_{1-x}S$ nanocomposite with enhanced solar photocatalytic H_2-production performance. *Nano Lett.* 12: 4584-4589.

[4] Zoud A. H., Zaatar N., Saadeddin I., Ali C., Park D., Campet G., Hilal H. S., (2010), CdS-sensitized TiO_2 in phenazopyridine photo-degradation: Catalyst efficiency, stability and feasibility assessment. *J. Hazard. Mater.* 173: 318-325.

[5] Lin Y. F., Song J., Ding Y., Lu S. Y., Wang Z. L., (2008), Piezoelectric nanogenerator using CdS nanowires. *Appl. Phys. Lett.* 92: 022105-022107.

[6] Lin Y. F., Song J., Ding Y., Lu S. Y., Wang Z. L., (2008), Alternating the output of a CdS nanowire nanogenerator by a white-light-stimulated optoelectronic effect. *Adv. Mater.* 20: 3127-3130.

[7] Williams R., Yocom P. N., Stofko F. S., (1985), Preparation and properties of spherical zinc sulfide particles. *J. Colloid Interface Sci.* 106: 388-398.

[8] Thompson A. H., (1975), The verification of the existence of TiS_2. *Mater. Res. Bull.* 10: 915-919.

[9] Xiong S., Xi B., Wang C., Zou G., Fei L., Wang W., Qian Y., (2007), Shape-controlled synthesis of 3D and 1D structures of CdS in a binary solution with L-Cysteine's assistance. *Chem. A Eur. J.* 13: 3076-3081.

[10] Gai H., Wu Y., Wu L., Wang Z., Shi Y., Jing M., Zou K., (2008), Solvothermal synthesis of CdS nanowires using L-Cysteine as sulfur source and their characterization. *Appl. Phys. A Mater. Sci. Pro.* 91: 69-72.

[11] El-Menyawy E. M., Zedanb I. T., Azab A. A., (2017), One-pot solvothermal synthesis and characterization of CdS nanotubes decorated with graphene for solar cell applications. *J. Alloys Comp.* 695: 3429-3434.

[12] Murugan A. V., Kale B. B., Kulkarni A. V., Kunde L. B., Saaminathan V., (2005), Novel approach to control CdS morphology by simple microwave-solvothermal method. *J. Mater. Sci. Mater. Electron.* 16: 295-299.

[13] Kozhevnikova N. S., Gyrdasova O. I., Vorokh A. S., Baklanova I. V., Buldakova L. Y., (2014), A facile route of coupling of ZnO nanorods by CdS nano particles using chemical bath deposition. *Nanosystems: Phys. Chem. Mathem.* 5: 579–589.

[14] Tiwari R., Dubey V., Tamrakar R. K., (2013), Copper doped cadmium sulphide (Cds : Cu) quantum particles: Topological, morphology and photoluminescence studies. *Int. J. Ind. Eng. Tech.* 3: 67-74.

[15] John Xavier R., Angelin Prema A., Arockia Sahayaraj P., Pragathiswaran C., Dharmalingam V., (2016), The properties of chemical bath deposited cadmium sulfide thin films with the effect of ammonia salt concentration. *Adv. Appl. Sci. Res.* 7: 178-182.

[16] Kawar S. S., Pawar B. H., (2009), Synthesis and characterization of CdS n-type of semiconductor thin films having nanometer grain size. *Chalcog. Lett.* 6: 219-225.

[17] Li Y., Liao H., Ding Y., Fan Y., Zhang Y., Qian Y., (1999), Solvothermal elemental direct reaction to CdE (E = S, Se, Te) semiconductor nanorod. *Inorg. Chem.* 38: 1382-1387.

[18] Im S.-J., Chae W.-S., Lee S.-W., Kim Y.-R., (2006), Novel rosette-shaped CdS microparticle with high surface area fabricated by lyotropic liquid crystal templating. *Mater. Res. Bull.* 41: 899-904.

[19] Han S., Lee M., Jeon J. Y., (2010), Formation of rosette-shaped Cd(II) thiolate coordination polymer in aqueous solution and conversion to CdS by calcination. *Bull. Korean Chem. Soc.* 31: 1091-1093.

[20] Wang Q., Pan D., Jiang S., Ji X., An L., Jiang B., (2005), A new two-phase route to high-quality CdS nanocrystals. *Chem. Eur. J.* 11: 3843-3848.

[21] Varfolomeev A., Zaretsky D., Pokalyakin V., Tereshin S., Pramanik S., Bandyopadhyay S., (2006), Admittance of CdS

nanowires embedded in porous alumina template. *Appl. Phys. Lett.* 88: 113114-113116.

[22] Long Y., Chen Z., Wang W., Bai F., Jin A., Gu C., (2005), Electrical conductivity of single CdS nanowire synthesized by aqueous chemical growth. *Appl. Phys. Lett.* 86: 153102-153104.

[23] Pan A., Liu R., Yang Q., Zhu Y., Yang G., Zou B., Chen K., (2005), Stimulated emissions in aligned CdS nanowires at room temperature. *J. Phys. Chem. B.* 109: 24268-24272.

[24] Ye C., Meng G., Wang Y., Jiang Z., Zhang L., (2002), On the growth of CdS nanowires by the evaporation of CdS nanopowders. *J. Phys. Chem. B.* 106: 10338-10341.

[25] Thongtem T., Phuruangrat A., Thongtem S., (2008), Characterization of nano- and micro-crystalline CdS synthesized using cyclic microwave radiation. *J. Phys. Chem. Solid.* 69: 1346-1349.

[26] Paul G. S., Gogoi P., Agarwal P., (2006), Sacrificial template growth of CdS nanotubes from $Cd(OH)_2$ nanowires. *J. Solid State Chem.* 179: 96-102.

[27] Lee M., Han S., Jeon Y. J., (2010), pH-controlled hydrothermal synthesis of submicrometer-sized CdS spheres with uniform size distribution. *Bull. Korean Chem. Soc.* 31: 3818-3821.

[28] Vaquero F., Fierro J. L. G., Yerga R. M. N., (2016), From nanorods to nanowires of CdS synthesized by a solvothermal method: Influence of the morphology on the photoactivity for hydrogen evolution from water cell applications. *Molecules.* 21: 401-417.

[29] Nie Q., Yuan Q., Chen W., Xu Z., (2004), Effects of coordination agents on the morphology of CdS nanocrystallites synthesized by the hydrothermal method. *J. Cryst. Growth.* 265: 420-424.

[30] Zhang H., Ma X., Ji Y., Xu J., Yang D., (2003), Single crystalline CdS nanorods fabricated by a novel hydrothermal method. *Chem. Phys. Lett.* 377: 654-657.

[31] Chen M., Pan L., Cao J., Ji H., Ji G., Ma X., Zheng Y., (2006), Synthesis of CdS nanoplates by PAA-assisted hydrothermal approach. *Mater. Lett.* 60: 3842-3845.

[32] Zhao H., Douglas E. P., Harrison B. S., Schanze K. S., (2001), Preparation of CdS nanoparticles in salt-Induced block copolymer micelles. *Langmuir.* 17: 8428-8433.

[33] Salavati-Niasari M., Davar F., Loghman-Estarki M. R., (2009), Long chain polymer assisted synthesis of flower-like cadmium sulfide nanorods via hydrothermal process. *J. Alloys Compd.* 481: 776-780.

[34] Karami H., Kaboli A., (2010), Pulsed current electrochemical synthesis of cadmium sulfide nanofibers. *Int. J. Electrochem. Sci.* 5: 706-719.

[35] Su J., Zhang T., Li Y., Chen Y., Liu M., (2016), Photocatalytic activities of copper doped cadmium sulfide microspheres prepared by a facile ultrasonic spray-pyrolysis method. *Molecules.* 21: 735-739.

[36] Kadash E. A., Al Hattami A. A., Rathod J. R., Patel K. D., Pathak V. M., (2014), Synthesis and characterization of cadmium sulfide crystals grown by DVT technique. *Int. J. Pure Appl. Sci. Technol.* 22: 18-26.

[37] Fulari V. J., Chougale U. M., Powar A. S., Tikone S. V., Shinde S. K., Lohar G. M., Thombare J. V., (2014-2015), Synthesis and characterization of Copper doped Cadmium Sulphide thin films by electrodeposition method. *J. Shivaji Uni. (Science & Technology).* 41: 2 pages.

[38] Raoof L. M., Dakhil O. A., Dagher H. F., (2016), Preparation of cadmium sulfide nanoparticles by laser ablation in methanol solution. *J. Multidisc. Eng. Sci. Stud.* 2: 579-582.

[39] Shri Prasad S., Madhavan J., (2013), Synthesis and characterization of CdS quantum dots by reverse micelles method. *Der. Pharma. Chem.* 5: 1-4.

[40] Kumar E., Rajasekaran S., Muthuraj D., (2014), Preparation and characterization of polyaniline/cadmium sulfide (Pani/CdS) nanocomposite via in-situ polymerization. *Int. J. Rec. Sci. Res.* 5: 1491-1494.

[41] Hanifehpour Y., Hamnabard N., Mirtamizdoust B., Joo S. W., (2016), Sonochemical synthesis, characterization and sonocatalytic performance of terbium-doped CdS nanoparticles. *J. Inorg. Organomet. Polym.* 26: 623-631.

[42] Khodadadeh F., Aberoomand Azar P., Tehrani M. S; Assi N., (2016), Photocatalytic degradation of 2, 4, 6-Ttrichlorophenol with CdS nanoparticles synthesis by microwave-assisted sol-gel method. *Int. J. Nano Dimens.* 7: 263-269.

[43] Yoshimura M., Byrappa K., (2008), Hydrothermal processing of materials: Past, present and future. *J. Mater. Sci.* 43: 2085-2103.

[44] Cao Y., Hu P., Jia D., (2013), Phase- and shape-controlled hydrothermal synthesis of CdS nanoparticles, and oriented attachment growth of its hierarchical architectures. *Appl. Sur. Sci.* 265: 771-777.

[45] Emadi H., Salavati-Niasari M., Sobhani A., (2017), Synthesis of some transition metal (M: ^{25}Mn, ^{27}Co, ^{28}Ni, ^{29}Cu, ^{30}Zn, ^{47}Ag, ^{48}Cd) sulfide nanostructures by hydrothermal method. *Adv. Colloid Interf. Sci.* 246: 52-74.

[46] Wei Q., Kang S. -Z., Mu J., (2004), Green synthesis of starch capped CdS nanoparticles. *Colloids Surf. A: Phys. Chem. Eng. Aspects*. 247: 125-127.

[47] Divya Rao M., Pennathur G., (2017), Green synthesis and characterization of cadmium sulphide nanoparticles from chlamydomonas reinhardtii and their application as photocatalysts. *Mater. Res. Bull.* 85: 64-73.

[48] Dumbrava A., Badea C., Prodan G., Ciupina V., (2010), Synthesis and characterization of cadmium sulfide obtained at room temperature. *Chalcogenide Lett.* 7: 111-118.

[49] Pascual J., Camassel J., Mathieu M., (1978), Fine structure in the intrinsic absorption edge of TiO_2. *Phys. Rev. B: Solid State.* 18: 5606-5614.

[50] Khan Z. R., Zulfequar M., Shahid Khan M., (2010), Optical and structural properties of thermally evaporated cadmium sulphide thin films on silicon (1 0 0) wafers. *Mater. Sci. Eng. B.* 174: 145-149.

[51] Kakodkar S. B., (2016), Synthesis, characterisation and photocatalytic activity of cadmium sulphide nanoparticles. *Chem. Sci. Trans.* 5: 75-78.